Label-Free Biomedical Imaging with High Sensitivity by Stimulated Raman Scattering Microscopy

Citation	Freudiger, Christian W., Wei Min, Brian G. Saar, Sijia Lu, Gary R. Holtom, Chengwei He, Jason C. Tsai, Jing X. Kang, and X. Sunney Xie. 2008. Label-free biomedical imaging with high sensitivity by stimulated Raman scattering microscopy. Science 322(5909): 1857-1861.
Published Version	doi:10.1126/science.1165758
Accessed	February 19, 2015 12:03:06 PM EST
Citable Link	http://nrs.harvard.edu/urn-3:HUL.InstRepos:10875726
Terms of Use	This article was downloaded from Harvard University's DASH repository, and is made available under the terms and conditions applicable to Open Access Policy Articles, as set forth at http://nrs.harvard.edu/urn-3:HUL.InstRepos:dash.current.terms-of-use#OAP

Label-free biomedical imaging with high sensitivity by stimulated Raman scattering microscopy

Christian W. Freudiger *[,1,2]; Wei Min *[,1]; Brian G. Saar [1]; Sijia Lu [1]; Gary R. Holtom [1];

Chengwei He [3]; Jason C. Tsai [4]; Jing X. Kang [3]; X. Sunney Xie [1,#]

* contributed equally

[#] to whom correspondence should be addressed. E-mail: xie@chemistry.harvard.edu

[1] Department of Chemistry and Chemical Biology, Harvard University, Cambridge, MA 02138 (USA)

[2] Department of Physics, Harvard University, Cambridge, MA 02138 (USA)

[3] Department of Medicine, Massachusetts General Hospital and Harvard Medical School, Boston, MA 02114 (USA)

[4] Pfizer Global Medical, 685 3rd Ave, MS 1325, New York, NY 10017 (USA)

Summary

Chemical imaging based on stimulated Raman scattering allows highly sensitive 3D mapping of distributions of metabolite and drug molecules in living cells and tissues.

Abstract

Label-free chemical contrast is highly desirable in biomedical imaging. Spontaneous Raman microscopy provides specific vibrational signatures of chemical bonds, but is often hindered by low sensitivity. Here we report a 3D multiphoton vibrational imaging technique based on stimulated Raman scattering (SRS). The sensitivity of SRS imaging is significantly greater than that of spontaneous Raman microscopy, which is achieved by implementing high-frequency (MHz) phase-sensitive detection. SRS microscopy has a major advantage over previous coherent Raman techniques in that it offers background-free and readily interpretable chemical contrast. We show a variety of biomedical applications, such as differentiating distributions of omega-3 fatty acids and saturated lipids in living cells, imaging of brain and skin tissues based on intrinsic lipid contrast, and monitoring drug delivery through the epidermis.

Vibrational microscopies based on infrared absorption and Raman scattering (*1, 2*) have been employed as label-free contrast mechanisms based on characteristic frequencies of various chemical bonds. However, infrared microscopy has limited spatial resolution because of long infrared wavelengths. Spontaneous Raman scattering microscopy, while having higher spatial resolution due to shorter excitation wavelengths, is insensitive and thus often has limited imaging speed. Coherent anti-Stokes Raman scattering (CARS) microscopy offers higher sensitivity than spontaneous Raman microscopy (*3, 4*). However, a CARS spectrum is different from its corresponding spontaneous Raman spectrum due to a nonresonant background, which complicates spectral assignment, causes difficulties in image interpretation, and limits detection sensitivity.

Here we explore stimulated Raman scattering (SRS) as an imaging contrast mechanism. SRS is analogous (*5, 6*) to the well-known phenomenon of stimulated emission (*7*), and was first observed in 1962 (*8*). It has been used in many spectroscopic studies (*9-12*). In spontaneous Raman scattering, only one laser beam at a frequency ω_p illuminates the sample and the signal is generated at the Stokes and anti-Stokes frequencies, ω_S and ω_{AS} respectively, due to inelastic scattering. In SRS, however, two laser beams at ω_p and ω_S coincide on the sample (Fig.1A). When the difference frequency, $\Delta\omega=\omega_p-\omega_S$, also called the Raman shift, matches a particular molecular vibrational frequency Ω, amplification of the spontaneous Raman signal is achieved by virtue of stimulated excitation. Consequently, the intensity of the Stokes, I_S, experiences a gain, ΔI_S, (stimulated Raman gain, SRG) and the intensity of the pump, I_p, experiences a loss, ΔI_p, (stimulated Raman loss, SRL), as shown in Fig.1B. In contrast, when $\Delta\omega$ does not match any vibrational resonance, SRL and

3

SRG cannot occur. Therefore, unlike CARS, SRL and SRG do not exhibit a nonresonant background (*11*).

The intensity of SRG or SRL is described by $\Delta I_S \propto N \cdot \sigma_{Raman} \cdot I_p \cdot I_S$ and $\Delta I_p \propto - N \cdot \sigma_{Raman} \cdot I_p \cdot I_S$, where N is the number of molecules in the probe volume and σ_{Raman} is the molecular Raman scattering cross-section (*6*). As in other multi-photon techniques (*3, 13*), the nonlinearity of SRL and SRG in the overall excitation intensity allows 3D sectioning. Such nonlinear excitation is typically accomplished by picosecond or femtosecond pulse trains in the near-infrared region.

SRS as a contrast mechanism for microscopy has been recently reported using multiplex detection with a photodiode array in combination with a femtosecond amplified laser system (*14*). While the amplified laser system generates a large SRS signal, it is not suitable for bioimaging because the excessive peak power causes sample damage (*15*) and the low repetition rate limits the image acquisition speed.

We take a different approach using high repetition rate (76MHz) picosecond pulse-trains with four orders of magnitude lower peak power. The pump beam for SRL is provided by a synchronously pumped, tunable optical parametric oscillator (OPO) and the Stokes beam is provided by a 1064 nm modelocked Nd:YVO$_4$ oscillator. A 7ps pulse-width is chosen because its frequency bandwidth offers optimal spectral resolution (3cm^{-1}). Under this excitation condition, the small SRL and SRG signals ($\Delta I_p/I_p$ and $\Delta I_S/I_S < 10^{-4}$) are buried in the laser noise. Realizing that laser noise occurs primarily at low frequencies, we implement a high-frequency phase-sensitive detection scheme (*16, 17*). For SRL we modulate the intensity of the Stokes beam at 1.7MHz and detect the resulting intensity

modulation of the pump beam at the same frequency with a lock-in amplifier (Fig. 1C).

Similarly, SRG can be measured by modulating the pump beam and detecting the Stokes

beam (*18*). With this approach, $\Delta I_p/I_p < 10^{-7}$ can be achieved with a 1s time constant. To

acquire images via beam scanning, we used a 300µs time constant and a pixel dwell time of

170µs. We note that it is difficult to incorporate such phase-sensitive detection at radio

frequency (MHz) with a multiplex detector such as a diode array and that our method is

four orders of magnitude more sensitive than the previous report (*14*).

We detected SRL instead of SRG because the responsivity of the photodiode used is

higher for the pump than for the Stokes beam. Collinear pump- and Stokes-beams are

focused with a high numerical aperture objective (N.A. = 1.2) onto a common focal spot

(Fig. 1D). Because SRL and SRG are measured at the same frequencies as the input fields,

phase matching is automatically fulfilled. This allows deconvolution with a point spread

function similar to fluorescence microscopy, and makes image interpretation simpler than

in the case of CARS (*19*).

In SRL, the spatial resolution is limited by diffraction and is similar to that of two

photon fluorescence. To detect the pump- or Stokes-beams in the forward direction, we

used a condenser with an N.A.=1.35, which is higher than that of the excitation objective,

in order to minimize unwanted background due to cross-phase-modulation, which can yield

spurious background (*20, 21*). Alternatively, backward (epi) detection is possible in turbid

samples because multiple scattering events redirect a significant portion of the forward

propagating pump and Stokes beams to the backward direction, which can be collected with

the same excitation objective lens (*22*). SRL or SRG spectra at a particular position in the sample can be recorded by automated OPO tuning.

We verified that SRL is linear in both the pump and Stokes intensities (*18*). Unlike the CARS signal that is proportional to the square of the concentration, the linear dependence of SRL on analyte concentration (Fig. 1E) allows straightforward quantitative analysis. The detection limit is 50μM for retinol solutions (Fig. 1E) and 5mM for methanol (*18*), with average laser power <40mW ($30MW/cm^2$) for each beam. Close to the shot noise limit, this sensitivity corresponds to about 3,000 retinol and 300,000 methanol molecules in focus, respectively, which has surpassed the detection limit reported for CARS microscopy (*23*).

We show in Fig. 1F the SRL, spontaneous Raman and CARS spectra of an isolated Raman peak of *trans*-retinol (*18*). While SRL and spontaneous Raman spectra are nearly identical, the CARS spectrum exhibits a nonresonant background independent of the Raman shift, and spectral distortion because of interference with the background (*24*). Good agreement between the SRL, SRG and spontaneous Raman spectra is also seen for spectra with multiple peaks (Fig. 1G) (*18, 25*). Thus SRS allows simple spectroscopic identification based on Raman literature, particularity in the "crowded" fingerprint region.

As the first application, we monitored the uptake of omega-3 fatty acids by living human lung cancer cells through SRL imaging and microspectroscopy (Fig. 2). Polyunsaturated omega-3 fatty acids, such as eicosapentaenoic acid (EPA), provide health benefits through mechanisms such as dampening inflammation, lowering blood triglyceride levels and inducing cancer cell apoptosis, but can only be obtained from the diet (*26*). As

6

shown in Fig 2A, unsaturated fatty acids exhibit a Raman band at 3015 cm^{-1}, attributable to the stretching mode of =C-H bond associated with C=C double bonds (*27*). The intensity of this 3015 cm^{-1} mode is approximately proportional to the number of C=C double bonds in the lipid molecule. In contrast, the 2920cm^{-1} peak intensity is found to be similar for all saturated and unsaturated fatty acids.

When cells are grown with 25µM EPA for 24 hours (*18*), lipid droplets (LDs) are visible when imaging at both 2920 cm^{-1} (Fig 2C) and 3015 cm^{-1} (Fig 2D) bands. In the absence of EPA in the culturing media, the cells have few LDs inside the cytoplasm due to the limited lipid supply (*18*). The SRL images show much stronger signal outside the LDs at 2920 cm^{-1} than at 3015 cm^{-1}, indicating that most of the fatty acids in the cells are saturated. We also conducted SRL microspectroscopy at specific positions inside the cell to identify the local chemical composition. The nucleus exhibits an SRL spectrum (blue in Fig 2B) similar to that of the saturated fatty acids, with negligible contribution at 3015 cm^{-1}, whereas LDs have a pronounced 3015 cm^{-1} peak (red in Fig 2B). No sign of photo-damage, such as plasma membrane blebbing (*15*), was observed even after repeated imaging of the same cell. Therefore we can use SRL spectral imaging and microspectroscopy to follow uptake of unsaturated fatty acids by living cells, opening possibilities to study lipid metabolism and its associated diseases.

Next, we present SRS tissue imaging without staining. Many stains are impossible to apply *in vivo*. Label-free optical techniques, such as optical coherence tomography and diffusive optical tomography, often do not offer chemical contrast, while autofluorescence is limited to a few chemical species. Strong SRL signal originates from the CH$_2$ stretching

vibration (2845cm^{-1}) of lipids in tissue, especially in the brain, where lipid-rich myelin sheaths surround axons, as was seen in CARS microscopy (*28*). Fig. 3A shows forward-detected SRL images of a fiber tract in the *corpus callosum* of a thin slice of mouse brain. We also demonstrate epi SRL imaging from a ~1mm thick slice of mouse brain (Fig. 3B), which clearly reveal individual neurons.

Skin imaging is another application of SRS microscopy. Fig.3C shows three individual SRL sections of mouse skin in the same area but at different depths, all with Δω tuned into 2845cm^{-1} (*18*). This highlights the three-dimensional capability and sub-cellular resolution of SRS in tissue. At a depth of 4μm, the SRL image shows the *stratum corneum*, which consists of polygonal cells and serves as the main protective layer of the body. This suggests that the intercellular space is rich in lipids. At a depth of 42μm, lipid-rich sebaceous glands can be identified in the dermis. The nuclei of the gland cells are dark spots due to the lack of lipids. At a depth of 105μm, the subcutaneous fat layer is clearly visible.

Fig. 3D compares on and off vibrational resonance SRL and CARS images of *stratum corneum*. When Δω is tuned from on-resonance (2845cm^{-1}) to off-resonance (2780cm^{-1}) of the CH_2 stretching mode, the SRL signal vanishes completely whereas the non-resonant CARS background still exhibits contrast that complicates image interpretation. We note that tissue autofluorescence does not interfere with the SRS. The absence of the nonresonant background in SRS reflects the major advantage over CARS imaging.

We also show the use of SRS to monitor drug delivery. Fluorescent labels are usually larger than drug molecules and may perturb their transport properties. Although confocal spontaneous Raman microspectroscopy has been used to obtain longitudinal penetration profiles, the lateral distribution is often compromised due to the long pixel dwell times (*29*). Here we show the mapping of the distribution of two compounds, dimethyl sulfoxide (DMSO), a skin penetration enhancer (*29*), and retinoic acid (RA), which is used to treat acne, wrinkles, photo-aging, and acute promyelocytic leukemia (*30*). According to Raman spectra (Fig. 4A), DMSO and RA have isolated vibrational resonances at 670cm^{-1} and 1570cm^{-1}, respectively.

As a hydrophilic molecule, DMSO penetrates the skin via the protein phase, so the DMSO image in the *stratum corneum* (Fig. 4B) shows inverse contrast compared to the lipid image in Fig. 3C. A depth profile shows detectable DMSO over more than 60 microns (Fig. 4C), and the hydrophilic interaction with the tissue is confirmed in the subcutaneous fat layer. Simultaneous two-color imaging tuned into lipid and DMSO (*18*) allows us to show that the DMSO is insoluble in the lipid structures (Fig. 4D). In contrast, RA, which is a hydrophobic molecule, penetrates via the lipid-rich intercellular space in the epidermis (Fig. 4E and F) after ultrasonciation of the tissue to enhance delivery (*18*). These results show that SRS offers a new approach for studying pharmacokinetics *in situ*.

As a label-free and sensitive imaging modality, SRS microscopy allows mapping of molecular species in 3D and following their dynamics in living cells and organisms based on the wealth of Raman spectroscopy.

Citations

1.   C. V. Raman, K. S. Krishnan, *Nature* **121**, 711 (1928)

2.   G. Turrell, J. Corset, *Raman microscopy: developments and applications* (Academic Press, 1996)

3.   A. Zumbusch, G. R. Holtom, X. S. Xie, *Phys Rev Lett* **82**, 4142 (1999)

4.   C. L. Evans, X. S. Xie, *Annu Rev Anal Chem* **1**, 27 (2008)

5.   N. Bloembergen, *Am J Phys* **35**, 989 (1967)

6.   R. W. Boyd, *Nonlinear Optics* (Academic Press Inc., 2003)

7.   A. Einstein, *Phys Z* **18**, 121 (1917)

8.   E. J. Woodbury, W. K. Ng, *P IRE* **50**, 2367 (1962)

9.   A. Owyoung, *Opt Commun* **22**, 323 (1977)

10.   B. F. Levine, C. V. Shank, J. P. Heritage, *IEEE J Quantum Elect* **15**, 1418 (1979)

11.   M. D. Levenson, S. S. Kano, *Introduction to Nonlinear Laser Spectroscopy* (Academic Press Inc., 1988)

12.   P. Kukura, D. W. McCamant, R. A. Mathies, *Annu Rev Phys Chem* **58**, 461 (2007)

13.   W. Denk, J. H. Strickler, W. W. Webb, *Science* **248**, 73 (1990)

14.   E. Ploetz, S. Laimgruber, S. Berner, W. Zinth, P. Gilch, *Appl Phys B-Lasers O* **87**, 389 (2007)

15.   Y. Fu, H. F. Wang, R. Y. Shi, J. X. Cheng, *Opt Exp* **14**, 3942 (2006)

16.   J. Ye, L. S. Ma, J. L. Hall, *J Opt Soc Am B* **15**, 6 (1998)

17.   D. Fu *et al.*, *Opt Lett* **32**, 2641 (2007)

18.   *Methods, additional results and videos are available as supporting materials on Science Online*

19.   E. O. Potma, W. P. de Boeij, D. A. Wiersma, *J Opt Soc Am B* **17**, 1678 (2000)

20.   K. Ekvall *et al.*, *J Appl Phys* **87**, 2340 (2000)

21.   *We note that another spurious background signal can arise from two-color two-photon absorption of the pump and Stokes beams. See also ref. (17)*

22.   C. L. Evans *et al.*, *P Natl Acad Sci USA* **102**, 16807 (2005)

23.   F. Ganikhanov, C. L. Evans, B. G. Saar, X. S. Xie, *Opt Lett* **31**, 1872 (2006)

24.   Y. R. Shen, *The Principle of Nonlinear Optics* (John Wiley & Sons Inc., 1984)

25.   *We note that subtle spectral differences between spontaneous Raman and SRS have been predicted theoretically. See:* P. Kukura, D. W. McCamant, R. A. Mathies, J Phys Chem A 108, 5921 (2004)

26.   J. X. Kang, *J Membrane Biol* **206**, 165 (2005)

27.   C. Heinrich *et al.*, *Opt Exp* **16**, 2699 (2008)

28.   H. F. Wang, Y. Fu, P. Zickmund, R. Y. Shi, J. X. Cheng, *Biophys J* **89**, 581 (2005)

29.   P. J. Caspers *et al.*, *Pharmaceut Res* **19**, 1577 (2002)

30.   P. C. M. Van De Kerkhof *et al.*, *J Dermatol Treat* **17**, 198 (2006)
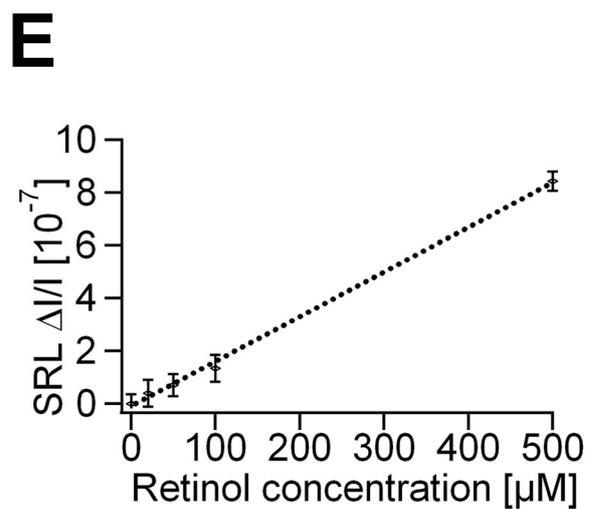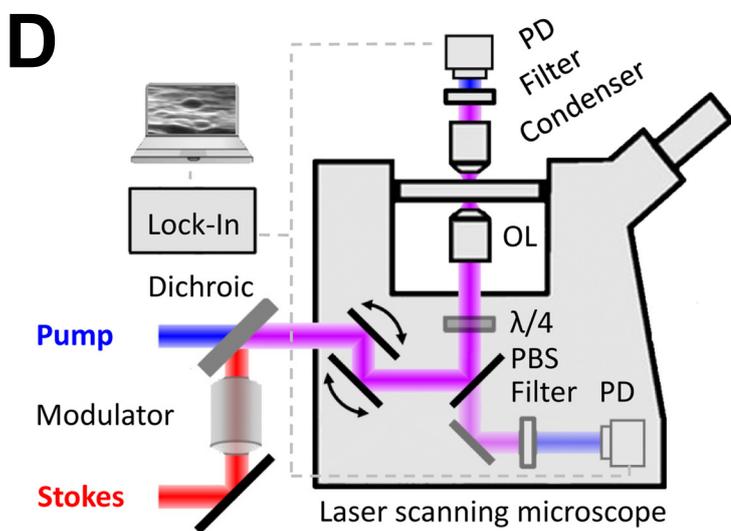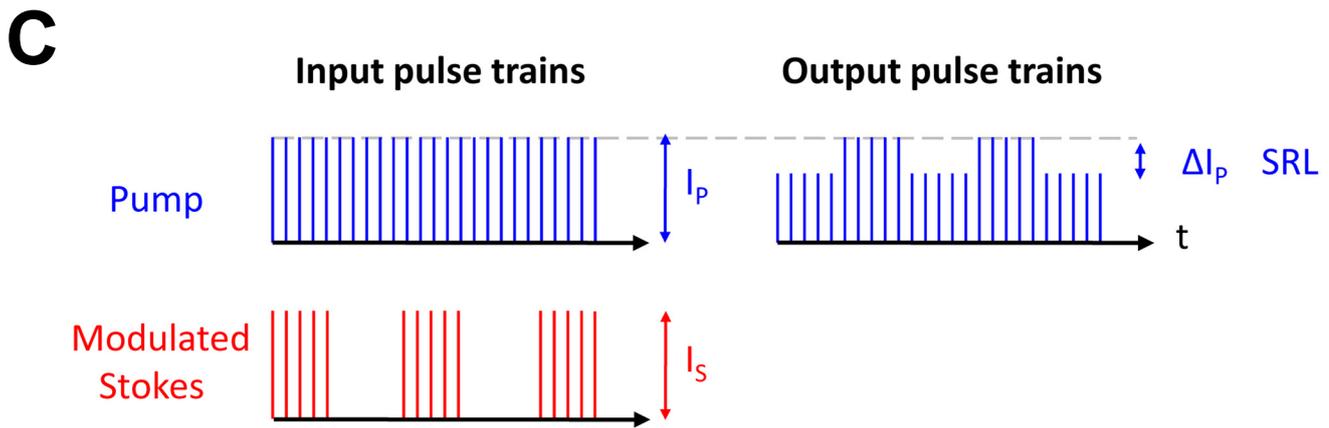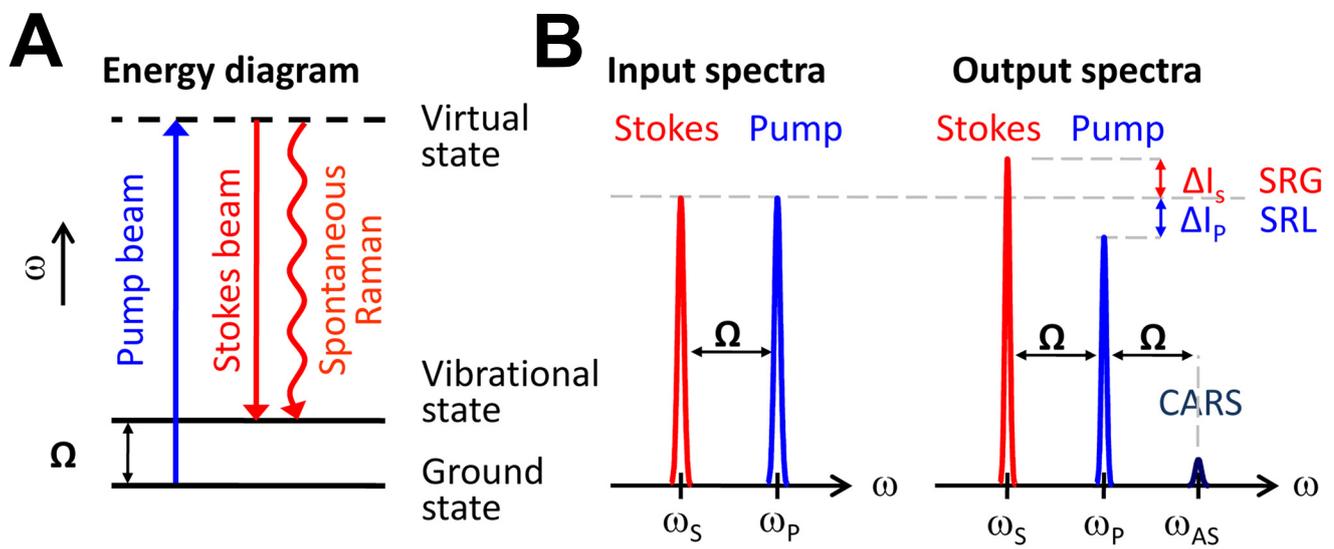
Figure Captions

Fig. 1. Principle and design of SRS microscopy. (A) Energy diagram for SRS. (B) Input and output spectra of SRS. SRS leads to an intensity increase in the Stokes beam (SRG) and an intensity decrease in the pump beam (SRL). Also shown (not to scale) is the CARS signal generated at the anti-Stokes frequency ω_{AS}. (C) SRL detection scheme. Stokes beam is modulated at high frequency (MHz), at which the resulting amplitude modulation of the pump- beam due to SRL can be detected. (D) SRL microscope with both forward and epi detection. The Stokes beam is modulated by an electro-optic modulator. The transmitted or reflected pump beam is filtered and detected by a large-area photodiode (PD). For epi detection, the back-scattered beams are collected by the excitation objective lens (OL) and separated from the excitation beams by a combination of a quarter wave plate ($\lambda/4$) and polarizing beam splitter (PBS). The SRL is measured by a lock-in amplifier to provide a pixel of the image. 3D images are obtained by raster-scanning the laser focus across the sample and microspectroscopy can be performed by automated tuning of the pump wavelength. (E) The linear dependence of SRL on concentrations of retinol in ethanol at 1595 cm^{-1}. Modulation depth $\Delta I_p/I_p < 10^{-7}$ can be achieved. Error-bars show one standard deviation of the signals for one minute recording. The detection limit was determined to be 50µM. (F) Agreement of SRL spectrum (red circles) with the spontaneous Raman spectrum (black line) of the Raman peak (1595 cm^{-1}) of 10 mM retinol in ethanol. The distorted CARS spectrum (blue squares) exhibits a typical dispersive shape. (G) The agreement of the more complex SRL spectrum of methanol (red circles) with the spontaneous Raman spectrum (black line).

Fig. 2. Omega-3 fatty acid uptake by A549 human lung-cancer cells monitored with SRL microscopy and microspectroscopy. (A) Spontaneous Raman spectra of docosahexaenoic acid (DHA, with 6 C=C bonds), eicosapentaenoic acid (EPA, with 5 C=C bonds), arachidonic acid (AA, with 4 C=C bonds) and oleic acid (OA, with single C=C bond). The strong Raman peak around 3015 cm^{-1} is characteristic of unsaturated fatty acids. (B) SRL spectra of a lipid droplet (LD, red line) and a region inside the nucleus (blue line). Unlike the nuclear region, the SRL spectrum of the LD shows good correspondence with the spectra from the pure EPA shown in (A). (C) SRL image of a cell at 2920cm^{-1}. (D) SRL image of the same cell at 3015 cm^{-1}. These findings indicate that EPA is taken up by the cells and stronger enriched in the LDs compared to other cellular organelles. No structural changes of the living cells due to photo-damage were observed after repeated scans.

Fig. 3. SRL imaging of fresh mouse tissue. (A) Neuron bundles in *corpus callosum* of mouse brain imaged at 2845cm^{-1} highlighting myelin sheaths rich in CH_2. (B) Epi-detected SRL CH_2 image acquired from thick brain tissue. (C) SRL CH_2 images of mouse ear skin in the same area at the indicated depths. From left to right: *stratum corneum* (4μm), sebaceous gland (42μm) and subcutaneous fat layer (105 μm). (D) Comparison of SRL and CARS images of *stratum corneum* on (2845cm^{-1}) and off (2780cm^{-1}) the CH_2 resonance. Unlike CARS, SRL has no nonresonant background.

Fig. 4. Monitoring drug delivery into fresh murine skin by SRS microscopy. (A) Raman spectra of dimethyl sulfoxide (DMSO, green), retinoic acid (RA, blue), and typical lipids in murine skin (red). (B) Top view of the penetrated DMSO (green) in the *stratum corneum* imaged at 670cm^{-1} with SRL. (C) SRL DMSO depth profile through the line in (B). (D)

Simultaneous two-color SRL image (18) of DMSO (670cm^{-1}, green) and lipid (2845cm^{-1}, red) in the subcutaneous fat layer at a depth of ~65 μm through the lower line in (C). (E) Top view of the penetrated RA (blue) in the *stratum corneum* imaged at 1570cm^{-1} with SRL. (F) SRL RA depth profile through the line in (E). SRS allows label-free 3D *in situ* visualization of two different drug delivery pathways into the skin.
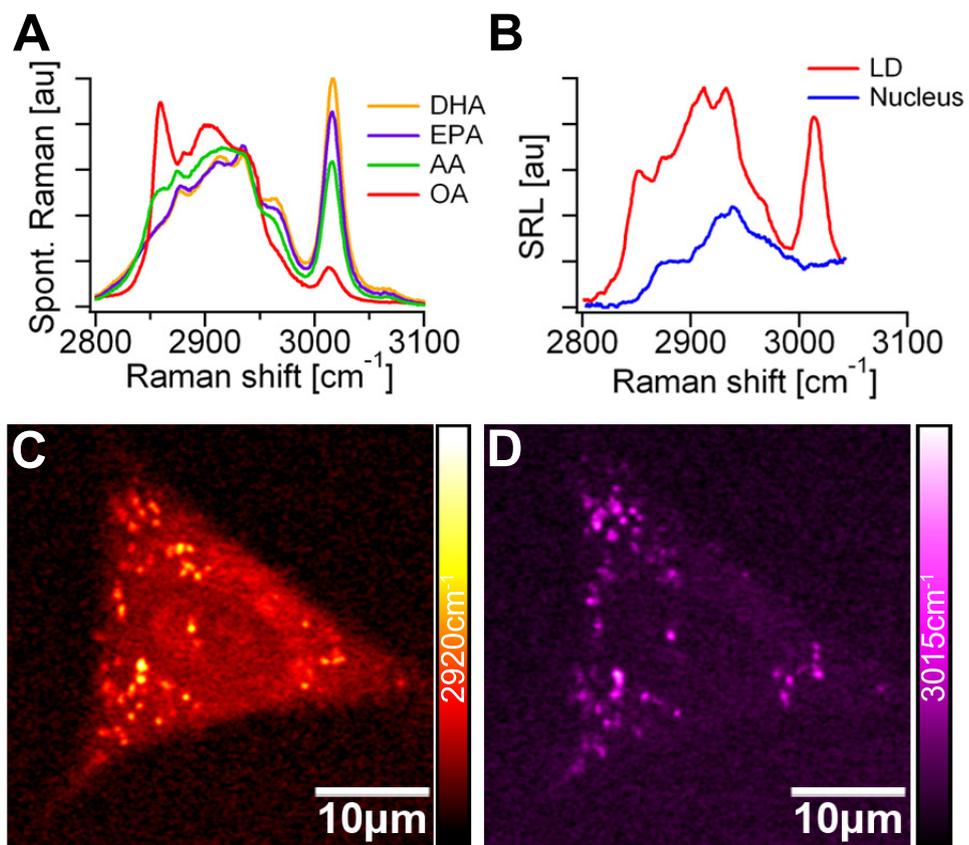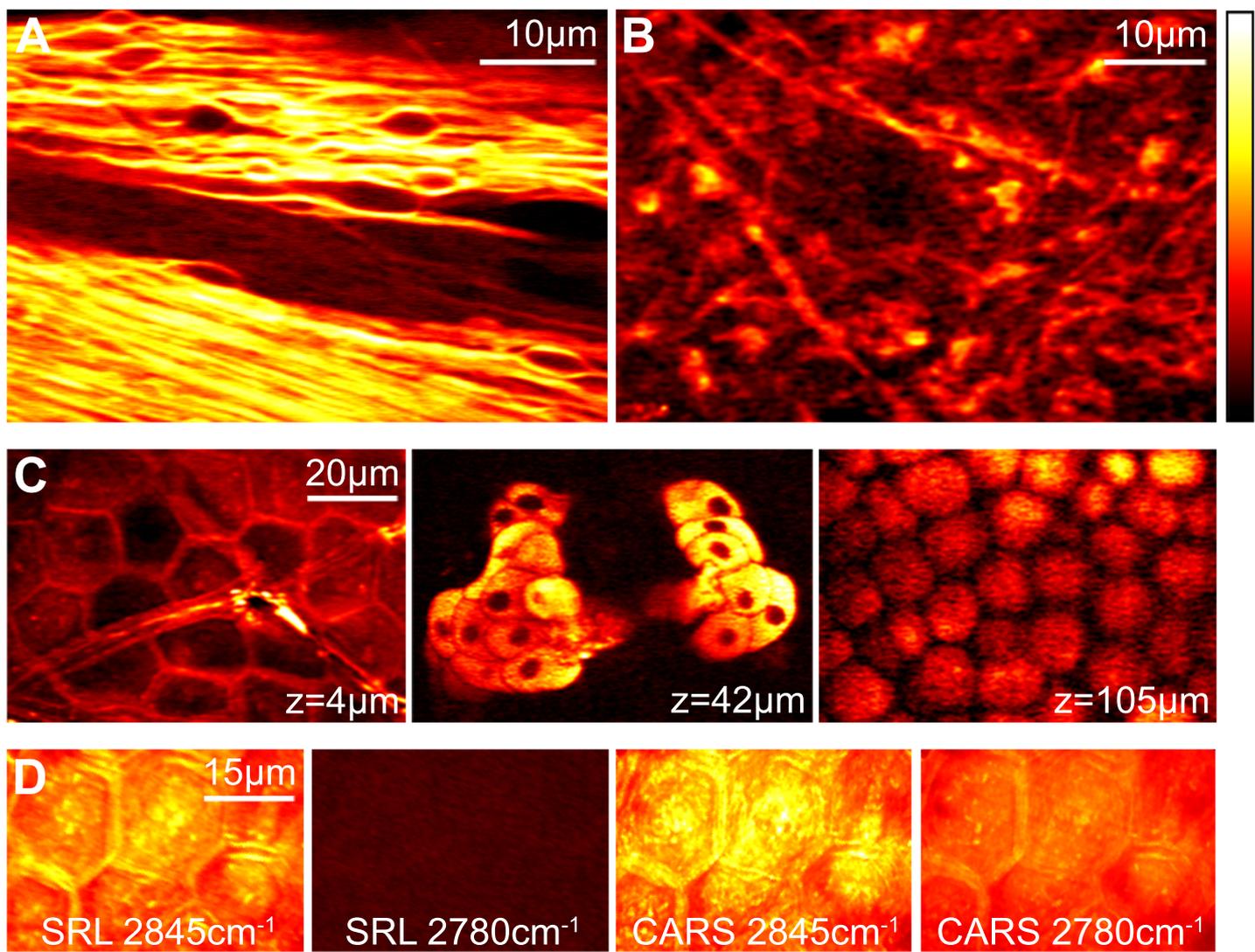
A Energy diagram

Virtual state

Pump beam — Stokes beam — Spontaneous Raman

ω

Ω

Vibrational state

Ground state

B Input spectra | Output spectra

Stokes — Pump

Ω

ω_S — ω_P — ω_{AS}

ΔI_S SRG

ΔI_P SRL

CARS

C Input pulse trains | Output pulse trains

Pump — I_P

Modulated Stokes — I_S

ΔI_P SRL

t

D

Lock-In

Dichroic

Pump

Modulator

Stokes

PD Filter Condenser

OL

$\lambda/4$

PBS Filter PD

Laser scanning microscope

E

SRL $\Delta I/I$ [10^{-7}]

Retinol concentration [μM]

F Raman shift [cm^{-1}]

Intensity [au]

— Raman
○ SRL
□ CARS

G Raman shift [cm^{-1}]

Intensity [au]

Figure 2

A 10μm

B 10μm

C 20μm z=4μm z=42μm z=105μm

D 15μm SRL 2845cm^{-1} SRL 2780cm^{-1} CARS 2845cm^{-1} CARS 2780cm^{-1}
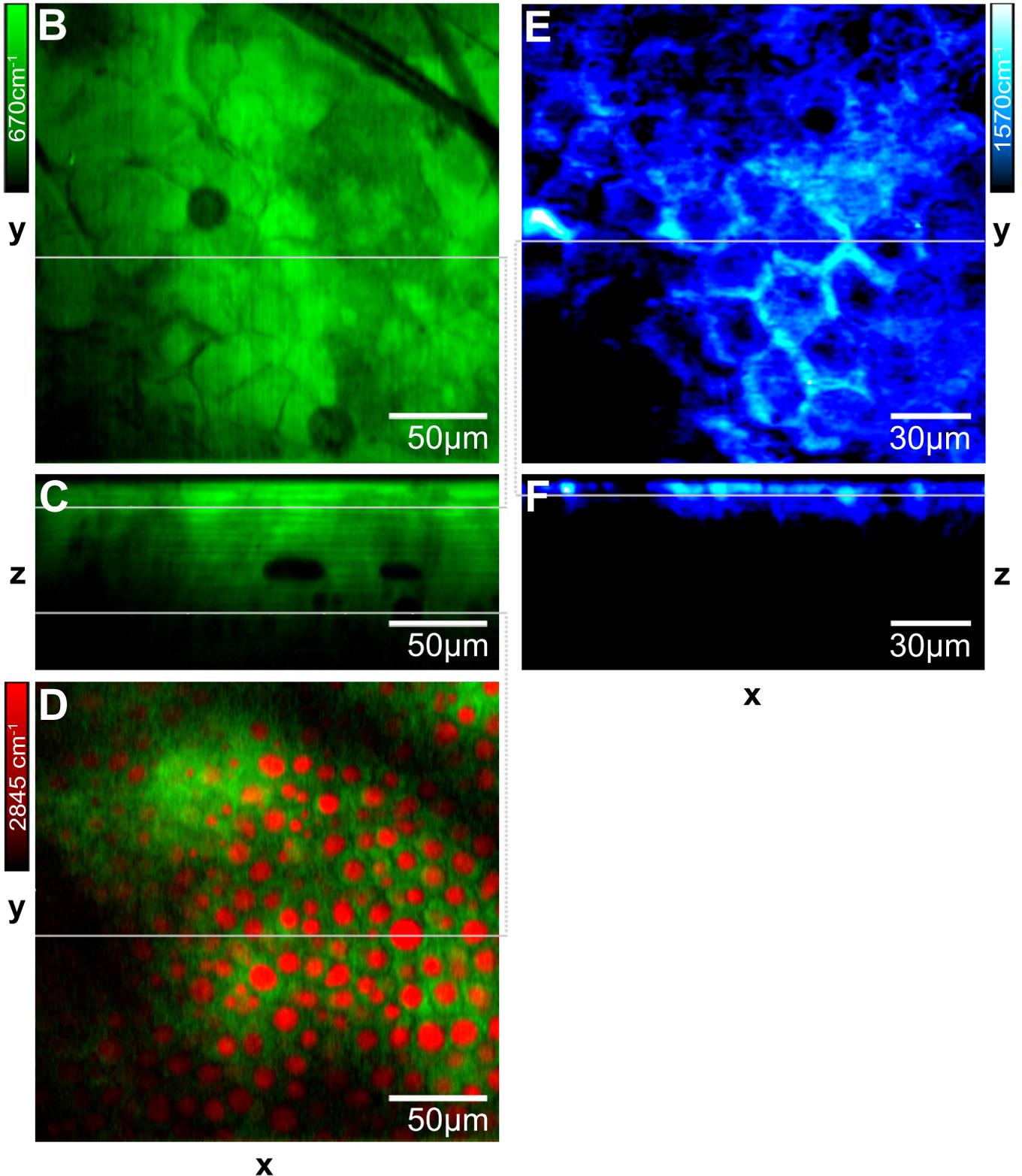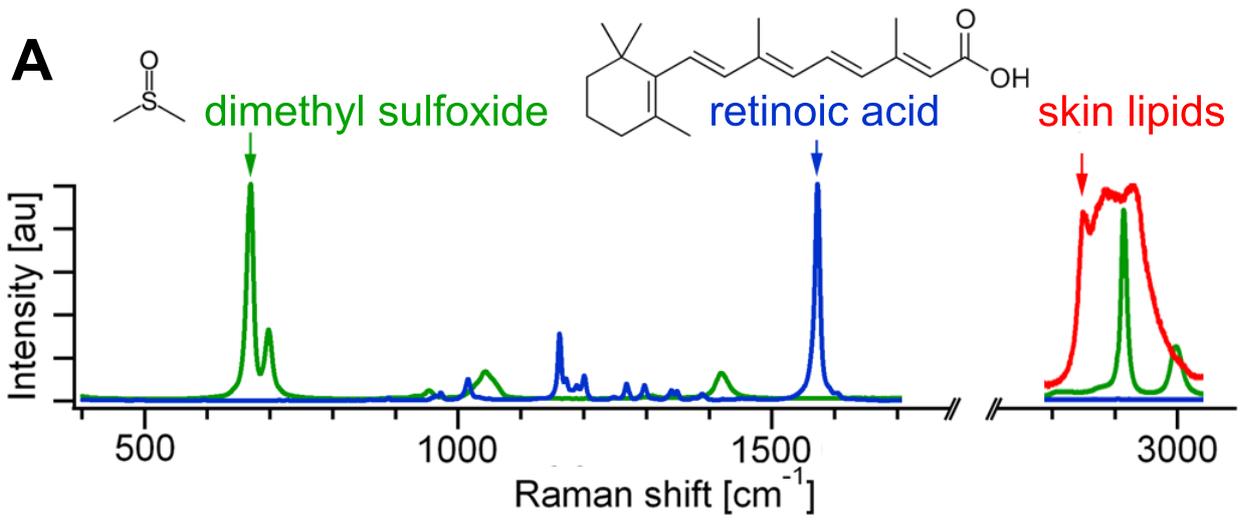
Figure 3

Figure 4

Supporting online materials

Methods

Detailed SRL Apparatus

Synchronized, mode-locked laser pulse-trains are provided by an optical parametric oscillator (OPO) (Levante Emerald, APE-Berlin) synchronously pumped by a frequency doubled Nd:YVO$_4$ laser (picoTRAIN, High-Q, 532nm, 7 ps, 76 MHz repetition rate). Additionally the pump-laser (picoTRAIN) provides a separated output of the fundamental beam (1064nm). The OPO uses a temperature-tuned non-critically phase matched LBO crystal. The coarse tuning of LBO temperature and the fine tuning of a stacked Lyot filter provide wavelength access to all Raman shifts from 500cm^{-1}-3400cm^{-1}. We utilized the signal-beam from the OPO as the pump-beam and the fundamental 1064nm-beam of the pump-laser as the Stokes-beam. The idler-beam of the OPO is blocked with an interferometric filter (Chroma Technology, CARS 890/220m). The pump beam is spatially overlapped with the 1064nm Stokes-beam with a dichroic beam-combiner (Chroma Technology, 1064 DCRB). Temporal overlap between pump and Stokes pulse trains is ensured with a delay-stage and measured with an autocorrelator (APE GmbH, PulseCheck).

The Stokes beam is modulated with a Pockel Cell (ConOptics, model 360-80) before entering the microscope. The 1.7MHz clock is provided to the driving electronics and the lock-in amplifier by a square-wave function-generator (Stanford Research Systems, DS345, Stanford Research Systems). Care is taken to provide proper RF-shielding. A polarization-analyzer is used to transform the polarization-modulation of the Pockel-Cell into amplitude-modulation. The analyzer is positioned after the dichroic beam-combiner to guarantee identical polarization of pump- and Stokes-beams. Modulation amplitude and DC offset of the RF-driver (ConOptics, model 25D) are adjusted to maximize the SRL signal from a pure compound tuned into vibrational resonance. Polarization-modulation instead of intensity-modulation is also possible in principle, as different tensor elements of the third-order nonlinear polarizability have different magnitude and would therefore generate an amplitude-modulation of the SRL signal. However the modulation-depth would be smaller for this approach, resulting in weaker signals. In addition, the average power in the focal spot is higher if polarization modulation is used.

Pump- and Stokes-beams are coupled into a modified laser scanning upright microscope (BX61WI/FV300, Olympus) optimized for near-IR throughput. For concentration studies and tissue imaging a 60x 1.2NA water (UPlanApo / IR, Olympus) and for cell imaging a 60x 1.1NA water dipping lens (LUMFI, Olympus) are used as excitation objectives. The beam-size is matched to fill the back-aperture of the objectives. Light is collected in transmission with a 60x 1.35NA oil objective (UPlanSAPO, Olympus) as condenser, which is aligned with white-light transmission

1

from a lamp. A telescope is used to image the scanning mirrors onto the photo-diode to avoid beam-movement due to laser scanning.

For epi-SRL imaging, a polarizing beam-splitter is positioned ~2cm before the excitation objective with its transmissive polarization direction parallel to the excitation pump and Stokes beams. Between this polarizing beam-splitter and the objective, an achromatic quarter-waveplate is inserted into the optical path with its fast axis at 45° with respect to the polarization direction of the excitation beams. Neglecting de-polarizing effects due to tissue scattering, after double passing the quarter-wave plate, the back-scattered light has a perpendicular polarization to the excitation light at the polarizing beam-splitter and thus is reflected to a custom-built side-port. A high OD band-pass filter (Chroma Technology, CARS 890/220m) is used to block the Stokes beam (at 1064nm) and transmit the pump-beam only. This filter works for imaging of all Raman-shifts from $500cm^{-1}$-$3400cm^{-1}$. No leak-through of the modulated Stokes-beam could be measured.

A large-area photodiode (FDS1010, Thorlabs) with reversed bias of 64V is used for detection of the pump beam. The output-current is low-pass filtered (Mini-Circuits, BLP-1.9+) to suppress the strong signal due to the laser pulsing (76MHz), and then terminated with 50Ω. A high-frequency lock-in amplifier (Stanford Research Systems, SR844RF) is used to demodulate the pump-intensity. The analog R (i.e. modulus) or x (i.e. in phase component)-output of the lock-in amplifier is fed into a modified input of the microscopy A/D-converter.

For the SRL spectral acquisition, we developed an RS232 computer control interface with the OPO in collaboration with APE GmbH (manuscript in preparation). In brief, we tuned the wavelength with the Lyot-filter within the phase-matching bandwidth of LBO crystal at a given temperature, allowing up to $300cm^{-1}$ tuning range. The microscope is set to point-scan, the OPO is tuned, and the intensity for each given $\Delta\omega$ is recorded. Intensity variations of the tuned pump-beam are corrected by simultaneously recording the pump-intensity with a photodiode. The compensation can be easily performed based on the linear power-dependence of SRL signal on pump beam intensity (Figure S3).
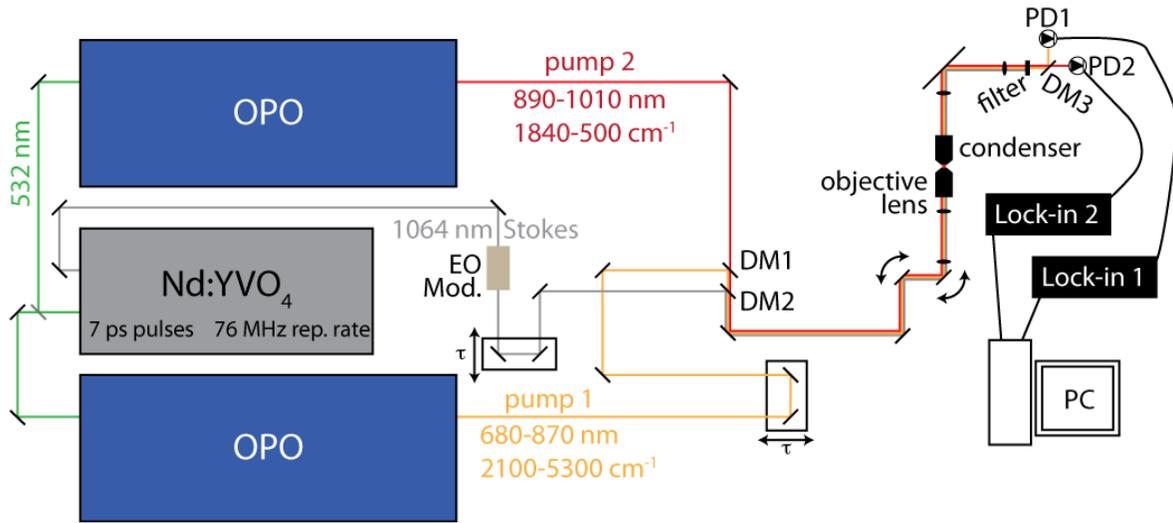
Simultaneous two color SRL imaging

Fig S1: A high power Nd:YVO$_4$ oscillator (High Q Laser, PicoTrain) provides 22 W of output power at 1064 nm with a 76 MHz repetition rate and 7 ps pulses. The majority of the output power is frequency doubled to produce a beam at 532 nm (~11W) which is split by a 50:50 beamsplitter and used to synchronously pump two optical parametric oscillators (OPOs) (APE GmbH, Levante Emerald). The Stokes beam for SRL is a portion of the undepleted 1064 nm fundamental from the Nd:YVO$_4$ oscillator, which is amplitude modulated by an electro-optic modulator (ConOptics). An acousto-optic modulator can also be used. Each of the OPOs provides an independently tunable beam which is used as the pump beam for the SRL process. The three beams are combined using two dichroic mirrors. DM1 is an 880 nm longpass mirror (Chroma Technology, 880 DCXR), which transmits pump 2 and reflects pump 1. This filter choice and the tuning range of signal beam of the OPO (680nm-1010nm) effectively limit the usable range of pump 2 to 890-1010 nm, and the usable range of pump 1 to 680 nm-870 nm. An optical delay stage allows the two pump beams to be overlapped in time. After the two pump beams are overlapped, they are combined with the Stokes beam (1064nm) on DM2 (Chroma Technology, 1064dcrb), which reflects 1064 nm and transmits below 1000 nm. An additional optical delay stage allows the Stokes beam to be overlapped in time with the two pump beams. The combined beams are coupled into a custom-modified laser scanning microscope as described above. After the collection optics, the two pump beams are then separated by DM3 (identical to DM1) and each beam is detected by a photodiode coupled to a lock-in amplifier as above. An additional narrowband optical filter may be supplied in front of each detector to reduce cross-talk between the channels. The two lock-in outputs are digitized on a PC to provide the simultaneously two-color image.

SRG imaging

     In SRG, the pump beam is modulated and the resulting amplitude modulation of the Stokes beam is detected (the opposite of SRL). In principle the SRL and SRG provide equivalent information, as shown in Fig. S4. To implement SRG, we placed an acousto-optic modulator (Crystal Technology, model 3080-122) in the pump beam and introduced an amplitude modulation at 10 MHz by modulating the RF power applied to the modulator. A set of 2 emission filters (Chroma Technology, D1125/150m) which blocked the ~800 nm pump laser beam and transmitted the 1064 nm Stokes beam were placed in front of the photodiode detector, and the signal was again processed by a lock-in amplifier. Because the responsivitiy of the silicon photodiodes that we use is higher for detection of the pump laser beam than for the Stokes beam, and because the collection optics more efficiently transmit the pump beam, SRL is preferred in our instrument and is used for all of the data shown in this report with the exception of Fig. S4. A schematic of the SRG detection scheme is shown in Fig. S2.
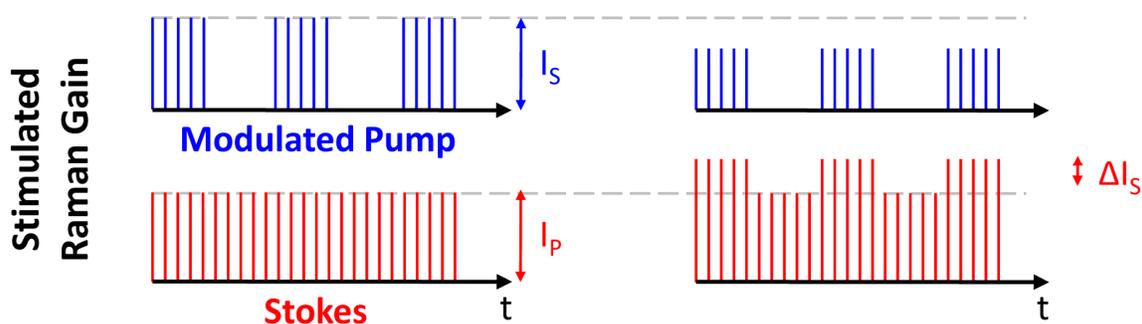

Fig. S2: Schematic of SRG. In SRG, the pump laser beam is amplitude modulated and the amplitude modulation is transferred into the Stokes beam as a gain in intensity due to the SRG process. This amplitude modulation of the Stokes beam can be detected by a lock-in amplifier. The SRG process only occurs when the difference between the pump and Stokes frequency is tuned into vibrational resonance with a molecular species in the sample volume.

Sample preparation concentration curves, spectra and power-dependence.

Methanol, ethanol and trans-retinol are used as purchased (Sigma Aldrich). Aqueous solutions are prepared with deionized water. Trans-retinol bottles are opened immediately before use. For spectral measurements and power dependence, we used sample chambers which were made from two cleaned No.1 coverslips separated by 120µm spacers (Grace Biolabs). For the concentration curve, we built a flow-cell from No.1 coverslips and a spacer to allow quick sample exchange without changing the sample-environment or focusing depth into the sample.

Sample preparation for live cell imaging

The human lung cancer cell line A549 was obtained from the American Type Culture Collection (ATCC, Rockville, MD). A549 cells are maintained in DMEM (Invitrogen, Carlsbad, CA, USA) supplemented with 5% fetal bovine serum (Invitrogen) at 37°C in a humidified 5% CO_2 air incubator. Cells are cultured on uncoated glass bottom dishes (P35G-1.0-14-C, MatTek Cooperation). First we image the control cells without adding EPA to the growth medium. For the uptake study, we add 25μM EPA into the growth medium, and cells are incubated for 24h in the 37°C incubator. After that, cells were taken out of the incubator and imaged under the microscope within 30min.

Sample preparation for tissue imaging & drug delivery

Tissue from wild-type, white mice are obtained from Dr. S. Kesari and coworkers at Dana Farber Cancer Institute (Boston, USA). Directly after sacrificing, the brain is removed from skull, and ear is removed. Tissue is transported in iced phosphate buffer and imaged within one hour after sacrificing. Brain slices are cut with a razor blade and sandwiched between two coverslips. Thin mouse ear can be imaged whole. No further sample preparation is needed.

For drug delivery experiments with DMSO and RA, mouse ear skin from white, wild-type mice was used. For DMSO delivery experiments, approximately 25 μl of a 20/80 v/v water/DMSO (Sigma Aldrich) mixture is pipetted onto the 5 x 5 mm piece of skin. The ear tissue is then incubated at 37° C and saturating humidity for one hour. The ~1-2 mm thick ear tissue is placed between two #1 coverslips and imaged using SRL at 670 cm^{-1} for DMSO and 2845 cm^{-1} for the endogenous skin lipids.

For retinoic acid delivery experiments, we found that penetration could be optimized by use of a commercially available sonication device that is marketed for transdermal drug delivery in human patients (SonoPrep, Sontra Medical Corp., Franklin, MA). We followed the manufacturer instructions to sonicate the mouse ear tissue. The tissue was removed from the animal and placed in the disposable foam target ring. The ear was cleaned with the recommended skin preparation pad (containing glycerin, methyl-paraben, propylparaben, benzyl alcohol, potassium sorbate, DMDM hydantoin and water) and the sonicator was placed over the sample. Coupling medium was applied to the sample, followed by a 30 s sonication period. After sonication, the excess coupling medium was blotted from the sample and 25 μl of a 2% retinoic acid in myritol (Sigma Aldrich) solution was pipetted onto the skin. Five minutes after drug application, the skin was blotted dry, placed between two #1 coverslips and imaged using SRL at 1570 cm^{-1} for retinoic acid.

Raman Spectroscopy

Spontaneous Raman spectra are acquired with a confocal Raman micro-spectrometer (LabRam HR800, Jobin Yvon) under 5mW 633nm He-Ne laser illumination, with 100x 0.9 NA air objective (MPlan, Olympus) and 10 minutes integration time. The spectrometer/CCD was calibrated with a characteristic line of Si at 520cm^{-1}.

5

Image progressing

Images are acquired with FluoView scanning software and processed using ImageJ (with UCSD plugins for microscopy), IgorPro and Photoshop. LUTs are applied in ImageJ. Graphs were made with IgorPro.
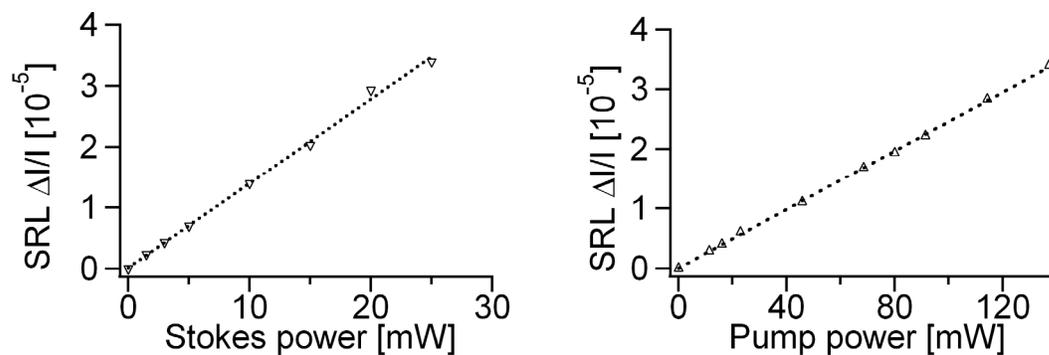
Results

Fig. S3: The power dependence of the SRL signal. The SRL signal is taken from 10% methanol/water solution tuned to the CH_3 stretching mode at 2840 cm^{-1}. The linear dependence of the signal on both pump beam and Stokes beam power is clear.
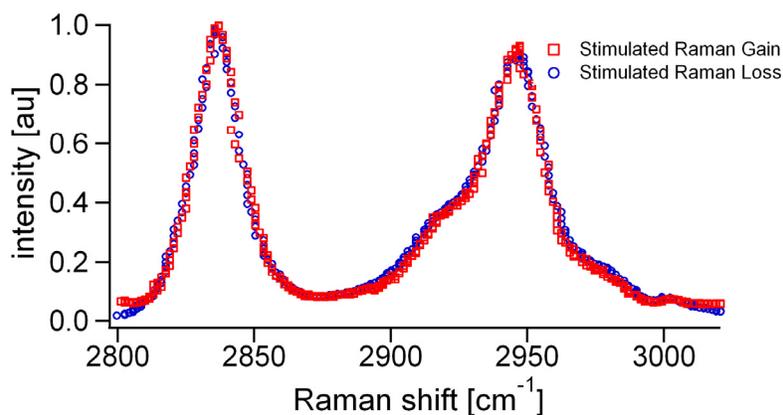

Fig. S4: SRL and SRG spectra of pure methanol tuned across the CH_3 stretching modes at 2840 cm^{-1} and 2950cm^{-1}. Within experimental uncertainty, these two spectra are identical as predicted by theory.
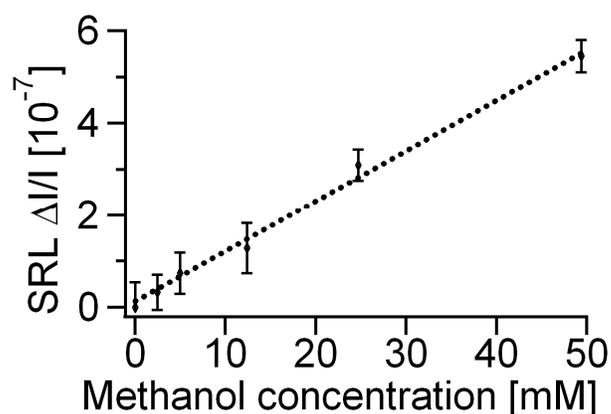
Fig. S5: Determination of methnol concentraton limit. For methanol, above, and Fig. 1E, data is sampled in the point-scan mode of the Olympus FluoView software as a time-trace, and the solutions with different concentrations are exchanged using a homemade flow cell and a syringe pump. Every concentration measurement is followed by a measurement of the zero-level (water). No significant change for water signal is found with increasing sample concentration. The lock-in signal is oversampled by the microscope A/D converter based on the time constants chosen. Time traces ~60 times longer than the time-constant are recorded. With this time trace, the average and standard deviation can be determined at each concentration level. In the concentration curve, the error-bars are determined from the standard deviation of the recorded SRL signals. With a signal-to-noise-ratio >1.6, the limit of detection is 5 mM and 50 μM for methanol/water and retinol/ethanol solutions, respectively, with laser intensities <40mW for each beam. This corresponds to approximately $3 \cdot 10^5$ methanol and 3,000 retinol molecules within the excitation focal volume (about 0.1 femto liter) of the microscope objective.
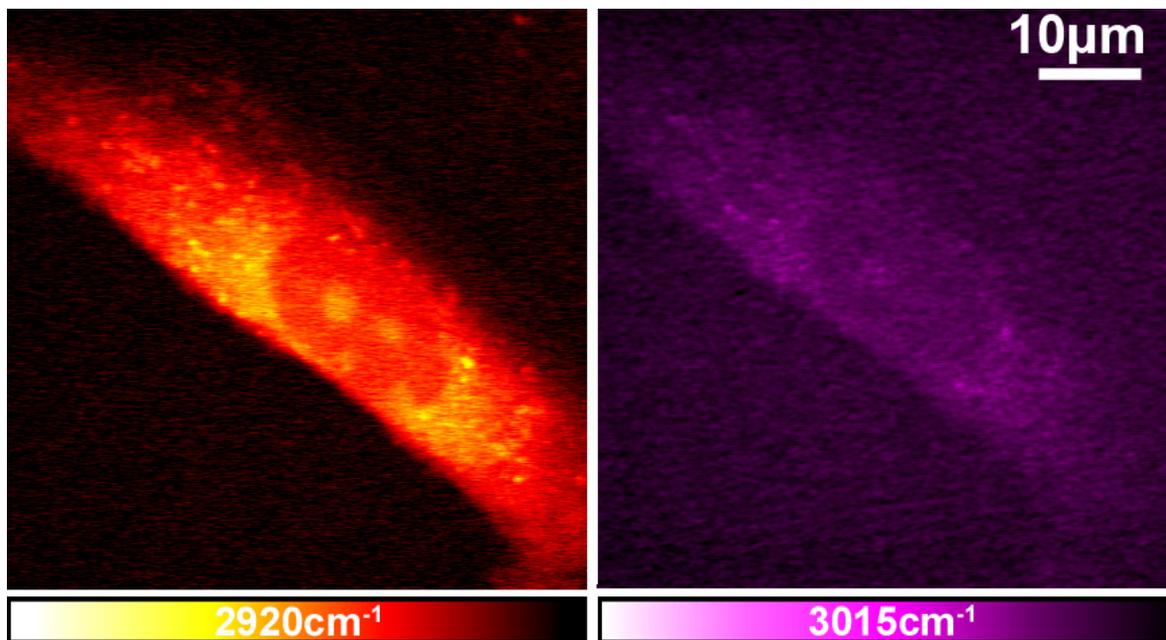
Fig. S6: Control A549 Cells. A549 human lung cancer cells are grown without adding EPA in the growth medium. SRL images at 2920 cm^{-1} (left) is much brighter than that at 3015 cm^{-1} (right), suggesting that most of the fatty acids inside cells are saturated. Also, fewer lipid droplets can be seen in the cytoplasm of these control cells due to the restricted lipid supply.

Movies

SRLmicroscopyBrain.avi: Movie shows three-dimensional image stack acquired with SRL microscopy in brain. CH$_2$ contrast highlights myelin sheaths around neurons. Three dimensional sectioning capability of SRL microscopy is evident.

SRLmicroscopySkin.avi: Movie shows three-dimensional image stack acquired with SRL microscopy in brain. CH$_2$ contrast highlights lipid rich structures: inter-cellular space of stratum corneum, hair follicles in the viable epidermis and sebaceous gland in the dermis (structures are mentioned is the chronological order of the movie).

SRLmicroscopyDMSO.avi: Movie shows three-dimensional image stack acquired with simultaneous two color SRL microscopy in murine skin. DMSO is applied to the skin and contrast is obtained by tuning into the 670 cm^{-1} peak (green channel). Endogenous lipid contrast is obtained from the 2845 cm^{-1} peak (red channel). The movie covers a depth of approximately 80 μm from the surface and shows DMSO penetration via a hydrophilic pathway.